



## Enhancing visible light photocatalytic degradation performance and bactericidal activity of BiOI via ultrathin-layer structure

Zaiyong Jiang<sup>a</sup>, Xizhuang Liang<sup>a</sup>, Yuanyuan Liu<sup>a,\*</sup>, Tao Jing<sup>b</sup>, Zeyan Wang<sup>a</sup>, Xiaoyang Zhang<sup>a</sup>, Xiaoyan Qin<sup>a</sup>, Ying Dai<sup>b</sup>, Baibiao Huang<sup>a,\*</sup>

<sup>a</sup> State key Laboratory of Crystal Materials, Shandong University, Jinan 250100, PR China

<sup>b</sup> School of Physics, Shandong University, Jinan 250100, PR China

### ARTICLE INFO

#### Article history:

Received 15 December 2016

Received in revised form 19 February 2017

Accepted 29 March 2017

Available online 31 March 2017

#### Keywords:

BiOI

Ultrathin-layer

Two-dimensional

Photocatalyst

Degradation

### ABSTRACT

Hollow flower-like BiOI photocatalyst (h-BiOI) was obtained via a facile solvothermal method, which consists of ultrathin nanosheets with a thickness of about 2 nm. The structures and morphologies of as-prepared products were characterized by XRD and SEM and the absorption properties were determined by DRS. h-BiOI exhibit a more positive VB band than that of bulk BiOI (b-BiOI), which suggests a much stronger oxidation ability of the former. Therefore, h-BiOI displays completely degradation ability towards RhB under visible light irradiation while b-BiOI only decomposes RhB into segmental fragments under the same conditions. In addition, h-BiOI exhibits significantly higher antibacterial performances than b-BiOI under LED (470 nm) light irradiation. Besides the higher oxidation ability, the excellent photocatalytic activity of h-BiOI may be due to the ultrathin nanosheet, which takes less time for the photogenerated electrons and holes to reach the surface and therefore reduce their recombination.

© 2017 Published by Elsevier B.V.

## 1. Introduction

Over the past few years, semiconductor photocatalysis played an important role in solar energy conversion, environmental decontamination and the inactivation of microbe in water [1–5]. Many kinds of nano-scaled semiconductor photocatalysts, such as TiO<sub>2</sub> [6,7], MoO<sub>3</sub> [8], ZnO [9], Fe<sub>2</sub>O<sub>3</sub> [10], TaON [11], ZnTi-LDH [12], ZnAl-LDH [13], conducting polymer [14] have been discovered. In particular, TiO<sub>2</sub> is the most widely investigated photocatalysts, because it is environmentally friendly, capable of complete mineralization, low cost and nontoxic [15,16]. Nevertheless, the band gap of TiO<sub>2</sub> is 3.2 eV, which means TiO<sub>2</sub> can only absorb a small fraction of solar energy (<4%). This fact greatly limits the practical application of TiO<sub>2</sub> [17]. In order to take full advantage of the solar energy, various efficient visible-light-driven photocatalysts have been developed, such as CdS [18], oxide-modified nickel [19], BiOBr [20,21], and BiOI, etc. Among them, BiOI is considered to be one of the most prospective photocatalysts owing to its good photocatalytic activity under visible light irradiation [22]. Moreover, BiOI also have received more and more attention in bacteria decontamination in water, as it is nontoxic, low cost and environmentally

friendly [5]. BiOI displays a layered structure consisting of a layer of [Bi<sub>2</sub>O<sub>2</sub>]<sup>2+</sup> and double layers of iodine ions which are connected via the internal static electric fields [23]. The unique layered structure is advantageous to the separation of photogenerated electron-hole pairs. However, photocatalytic activity of BiOI is still slightly low, which does not meet the requirements of practical applications. Therefore, it is necessary to enhance the photocatalytic efficiency.

Till to now, many strategies have been proposed, for example doping, semiconductor composition, solid solutions, crystal-facet control, morphology control, and the deposition of noble metals, etc [22,24,25,26–31]. Among them, the morphology control receives more and more attentions. Especially, ultrathin-layer preparation is identified as a newly promising method for improving the photocatalytic efficiency. For example, nitrogen-doped carbon quantum dots (N-CQDs) modified atomically-thin BiOI nanosheets nanojunctions were proved to enhance the photocatalytic activity of BiOI [32]. In addition, the band gap of ultrathin-layer BiOI can be extended according to a recent report [33], which means that the oxidation ability would be improved. Moreover, as far as we know, the photo-generated holes (h<sup>+</sup>) are the reactive species in the disinfection system of BiOI [34]. If increasing the oxidation ability of the holes will enhance bactericidal activity of BiOI. However, to the best of our knowledge, current study about ultrathin-layer is limited. Therefore, further exploration is very valuable for both scientific research and practical applications.

\* Corresponding authors.

E-mail addresses: [yliu@sdu.edu.cn](mailto:yliu@sdu.edu.cn) (Y. Liu), [bbhuang@sdu.edu.cn](mailto:bbhuang@sdu.edu.cn) (B. Huang).

Herein, in our work, we realized the bulk preparation of hollow BiOI flower like structure consisting of ultrathin nanosheet via one-pot facile solvothermal method. The Mott-Schottky result suggests that the valence band of the h-BiOI is more positive than that of b-BiOI, which suggests a stronger oxidation ability of h-BiOI. As expected, h-BiOI displays not only complete degradation of RhB under visible light but also good antibacterial performance.

## 2. Experimental

### 2.1. Chemicals

All reagents used in this study were of analytical grade and were purchased from the Sinopharm Chemical Reagent Corporation (Shanghai, China), which used without further purification.

### 2.2. Solvothermal synthesis of h-BiOI and b-BiOI

$\text{Bi}(\text{NO}_3)_3 \cdot 5\text{H}_2\text{O}$  (20 mmol) or KI (20 mmol) were added to 40 mL of ethylene glycol at room temperature with continuous stirring. Afterwards, the two solutions were mixed together and continuously stirred for 2 h. The suspension was transferred into a 100 mL Teflon-lined stainless autoclave. The autoclave was heated and maintained at 433 K for 24 h, and then cooled down to room temperature naturally. The resulting precipitate was washed several times with deionized water and ethyl alcohol and dried at 333 K for 6 h in vacuum oven. The sample obtained was denoted as h-BiOI. The bulk BiOI was synthesized according to the reported method [35], which was denoted as b-BiOI.

### 2.3. Characterization

X-ray powder diffraction (XRD) analysis was carried out on a Bruker AXS D8 advance powder diffractometer with Cu  $\text{K}\alpha$ X-ray radiation. The morphology was observed by a scanning electron microscopy (SEM, Hitachi S-4800) with an accelerating voltage of 7.0 kV. Both transmission electron microscopy (TEM) and high-resolution transmission electron microscopy (HRTEM) measurements were carried out on a JEOL-2100 microscope. Raman spectra were recorded at room temperature using Horiba LabRAM HR system with laser excitation of 1064 nm. UV-vis diffuse reflection spectra (DRS) were measured on a Shimadzu UV 2550 recording spectrophotometer using  $\text{BaSO}_4$  as a reference. A Micromeritics ASAP 2020 analyzer was used to measure the Brunauer-Emmett-Teller (BET) surface areas of the samples at liquid nitrogen temperature.

### 2.4. Photocatalytic activity measurement and electrochemical performances

The photocatalytic experiments were carried out with RhB aqueous solution ( $20 \text{ mg L}^{-1}$ ). 100 mg photocatalysts was used for each experiment. A 350 W Xe arc lamp (PLS-SXE350, Beijing Trustech Co., Ltd.) was used as the light source with a 420 nm cut off filter. Prior to irradiation, all the photocatalysts were immersed in the RhB solution for 1 h under stirring in order to achieve the adsorption/desorption equilibrium in the dark. At the given time interval, the aqueous solution was withdrawn for monitoring the absorption intensity at 554 nm (the maximum absorption wavelength of RhB) to record the concentration of RhB solution.  $40 \text{ mg L}^{-1}$  RhB concentration was used to study the effects of reactive species due to the strong adsorption of h-BiOI. And *E. coli* has been used as model bacteria in this research.

Photocurrent measurement for the samples was carried out using a CHI 660C electrochemical workstation with a 350 W Xe arc lamp as the light source. 10 mg of sample was spin coated on the ITO

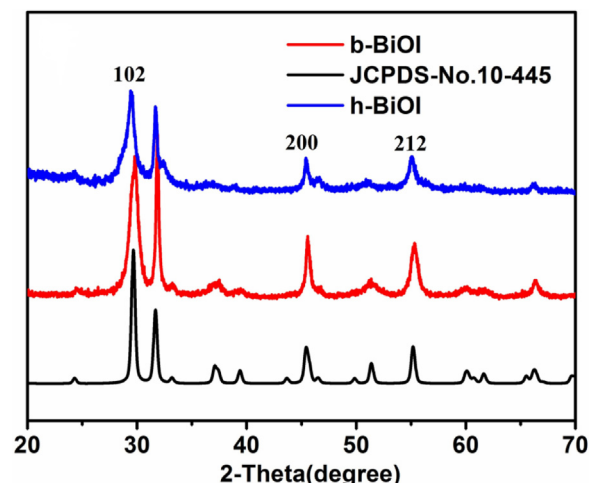


Fig. 1. XRD patterns of b-BiOI and h-BiOI.

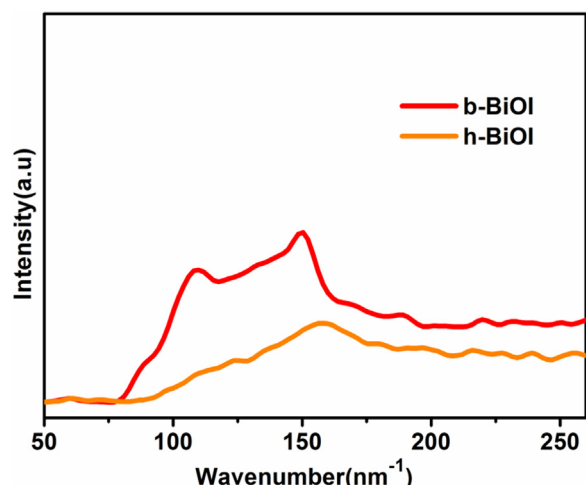


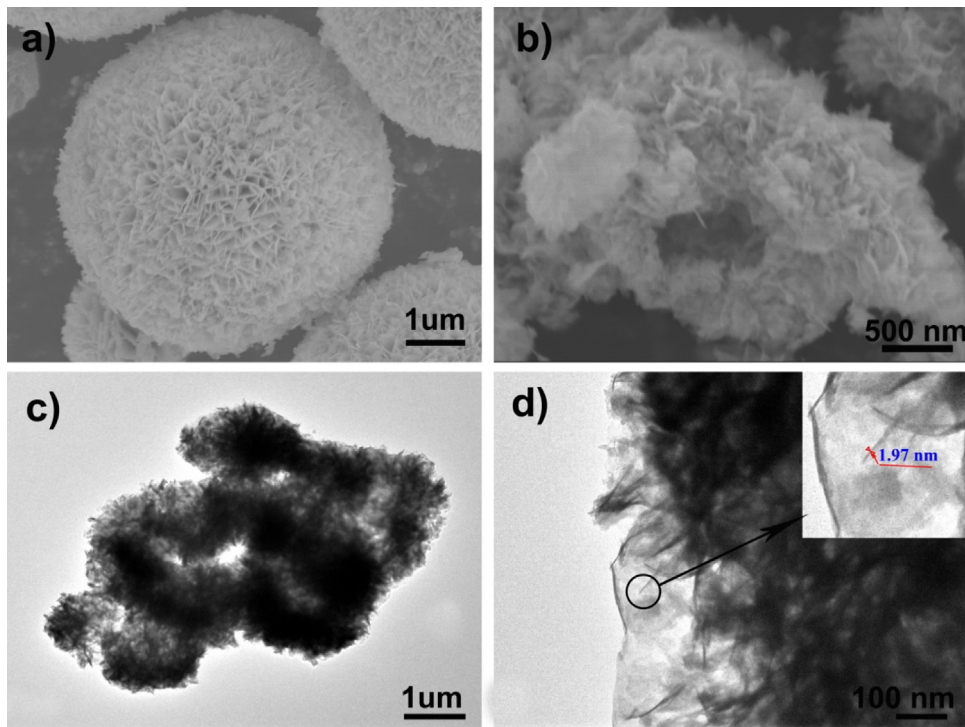
Fig. 2. Raman spectra for b-BiOI and h-BiOI.

glass electrode ( $1.5 \times 1.5 \text{ cm}^2$ ), which was served as working electrodes. Pt and saturated calomel electrode were used as the counter electrode and reference electrode, respectively. The  $\text{Na}_2\text{SO}_4$  solution (0.2 M) was employed as the electrolyte. The Mott-Schottky measurement was also performed.

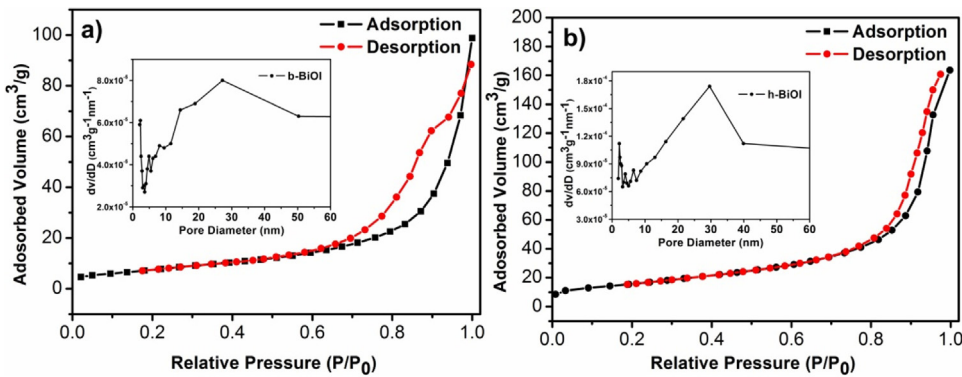
## 3. Results and discussion

Fig. 1b displays the XRD spectra of b-BiOI and h-BiOI. All diffraction peaks of the two samples could be perfectly assigned to the standard card of tetragonal BiOI (JCPDS No. 10-445). And, no extra diffraction peaks of impurities, such as  $\text{Bi}_2\text{O}_3$  or  $\text{Bi(OH)}_3$ , are detected. Moreover, it is observed that the peaks of h-BiOI indexed to the (102), (200) and (212) planes slightly shifted to low angle compared to that of b-BiOI, which could be ascribed to the ultrathin-layer.

Raman spectra were further investigated to find more structural information of h-BiOI. As is shown in Fig. 2, both samples show Raman band around  $150 \text{ cm}^{-1}$  were found, respectively, which could be assigned to  $\text{E}_g$  of Bi-I stretching mode [36]. h-BiOI displays a higher frequency than that of b-BiOI after careful check of this peak, which may be induced by the ultrathin-layer structure of h-BiOI. Besides that, a new peak at  $109.4 \text{ cm}^{-1}$  is observed for h-BiOI, which is absent for b-BiOI. This peak is most likely due to the surface in interface modes [37,38].



**Fig. 3.** SEM images of b-BiOI (a) and h-BiOI (b); TEM (c) and HRTEM (d) of h-BiOI.



**Fig. 4.** Nitrogen absorption–desorption isotherms of b-BiOI (a) and h-BiOI (b).

The SEM images of both h-BiOI and b-BiOI are shown in Fig. 3a–b. It can be seen that h-BiOI exhibit a hollow flower-like morphology, which consists of some interlaced nanosheets. The size of h-BiOI hollow flowers are about 1–2  $\mu\text{m}$ , while the size of b-BiOI is about 4–5  $\mu\text{m}$ . The TEM image (Fig. 3c) further confirms the SEM result, that is h-BiOI displays hollow structure. The HRTEM images (Fig. 3d) suggest that the nanosheets are nearly transparency, implying the ultrathin structure of nanosheet in b-BiOI. Through a closer observation for the vertical nanosheets (Fig. 3d), it is found that the ultrathin thickness is about 2 nm, confirming the ultrathin structure of h-BiOI. In contrast, the thickness of b-BiOI nanosheet is about 15 nm. (Fig. S1 in the SI)

It is well known that the surface area plays an important role in the photocatalytic property of the sample. A higher specific surface area could provide more active species on the surface and therefore more reactants are involved in the photocatalytic process, which in turn result in a higher photocatalytic efficiency. Generally speaking, hollow structure with ultrathin nanosheets would give rise to a big surface area. The nitrogen absorption–desorption isotherms of b-BiOI and h-BiOI are presented in Fig. 4. As expected, the BET surface

area of h-BiOI ( $58.23 \text{ m}^2/\text{g}$ ) is obviously higher than that of b-BiOI ( $28.39 \text{ m}^2/\text{g}$ ).

Fig. 5a displays the UV–vis DRS spectra of h-BiOI and b-BiOI. h-BiOI exhibits an obvious blue-shift compared to b-BiOI, which can be attributed to the ultrathin structure of h-BiOI. This is in good consistent with previous reports that ultrathin structure can extend the band gap [32]. Using the formula  $a\hbar\nu = A(\hbar\nu - E_g)^{n/2}$  [39], the band gaps  $E_g$  of b-BiOI and h-BiOI are determined to be 1.77 and 1.95 eV, respectively (Fig. S2). In addition, Mott–Schottky measurements of h-BiOI and b-BiOI are further investigated, from which the position of valence band (VB) can be determined. As shown in Fig. 5b, the VB position of h-BiOI (2.19 eV) is obvious positive shift compared with that of b-BiOI (1.99 eV). This result suggests that a stronger oxidation ability of h-BiOI than b-BiOI. Based on the combined results of DRS and Mott–Schottky plot, the conduction band (CB) positions of b-BiOI and h-BiOI are calculated to be 0.22 and 0.24 eV, respectively.

The visible light photocatalytic activities of the h-BiOI and b-BiOI were performed using RhB as the target molecule and the results are presented in Fig. 6a. As can be seen, only 40% percent of RhB molecules are decolorized over b-BiOI after 40 min irradiation.

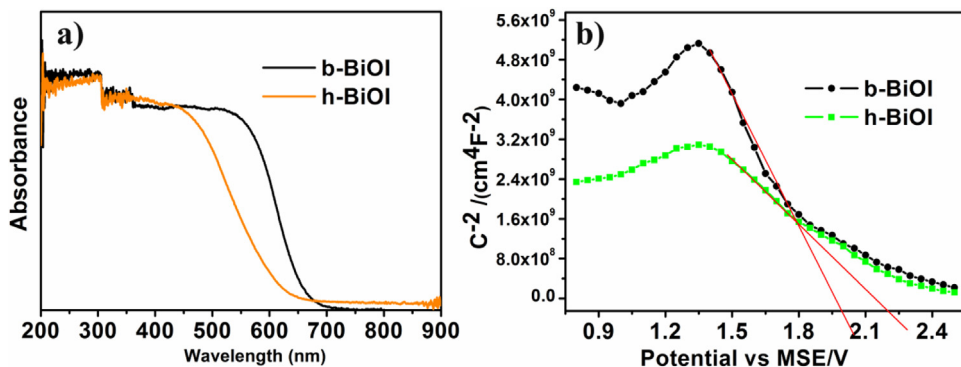


Fig. 5. UV-vis DRS spectra (a) and Mott-Schottky plot (b) of b-BiOI and h-BiOI.

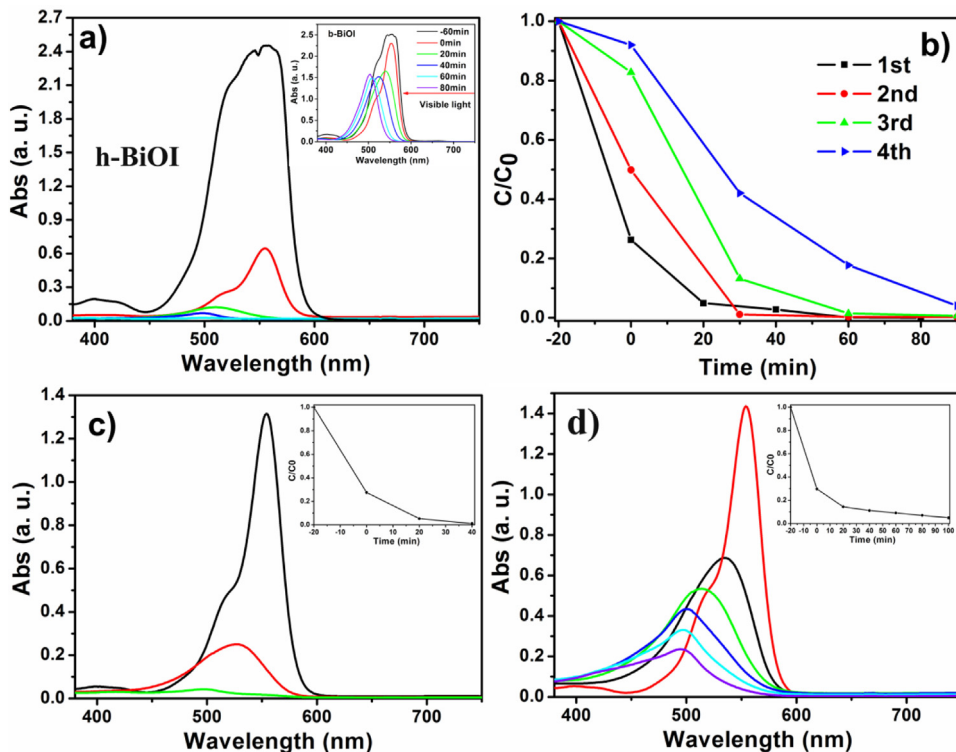


Fig. 6. (a) Photocatalytic degradation of RhB via h-BiOI and b-BiOI (inset), (b) Repeated photocatalytic degradation of RhB solution over h-BiOI as photocatalyst for four times, (c) and (d) The effects of reactive species in the photocatalytic degradation process of RhB using h-BiOI (c image, tert-butyl alcohol is used as the scavengers; d image, ammonium oxalate is used as the scavengers).

tion, and longer irradiation can not further degrade RhB. In contrast, 99.6% percent of RhB molecules are effectively decomposed over h-BiOI within 60 min. Obviously, h-BiOI displays significantly higher degradation efficiency than b-BiOI does. Furthermore, h-BiOI realizes the complete degradation of RhB molecules under visible light irradiation. This result is in consistent with the Mott-Schottky conclusions. In addition, h-BiOI displays a higher photocurrent than that of b-BiOI (Fig. S3 of the SI), suggesting that the ultrathin-layer is advantageous for the separation of photogenerated charge carriers. The photocurrent is in consistent with the photocatalytic results.

In order to further evaluate the cyclic degradation ability of h-BiOI (the ability of completely degrading the RhB molecules), repeated experiments were carried out, which are shown in Fig. 6b. The results exhibit that h-BiOI can still completely decompose RhB molecules after four times repeated experiments, though a slight decrease of photocatalytic activity is observed.

The active species during the photocatalytic process are checked using scavengers (tert-butyl alcohol is the scavengers of •OH,

ammonium oxalate is the scavengers of holes). As can be seen from Fig. 6c-d, the introduction of tert-butyl alcohol does not suppress the degradation of RhB while ammonium oxalate results in an obvious suppression. The results clearly indicate the photogenerated holes are the main active species under visible light irradiation. This result is in good consistent with more positive position of the valence band and the higher photocatalytic activity of h-BiOI. The disinfection activities of the photocatalyst towards *Escherichia coli* (*E. coli*) were investigated under LED (470 nm) irradiation. As shown in Fig. 7, h-BiOI displays significantly higher antibacterial performances than b-BiOI within 40 min. Control experiments of photocatalytic antibacterial performances, (1) without h-BiOI under LED (470 nm), and (2) without both h-BiOI and LED (470 nm), were further carried out (Fig. S4). Nearly no decrease of bacterial concentration was observed, suggesting the bactericidal activity is indeed due to the photocatalytic process of h-BiOI.

Based upon the experimental results, a possible mechanism for the higher photocatalytic activity of h-BiOI is proposed. As shown in

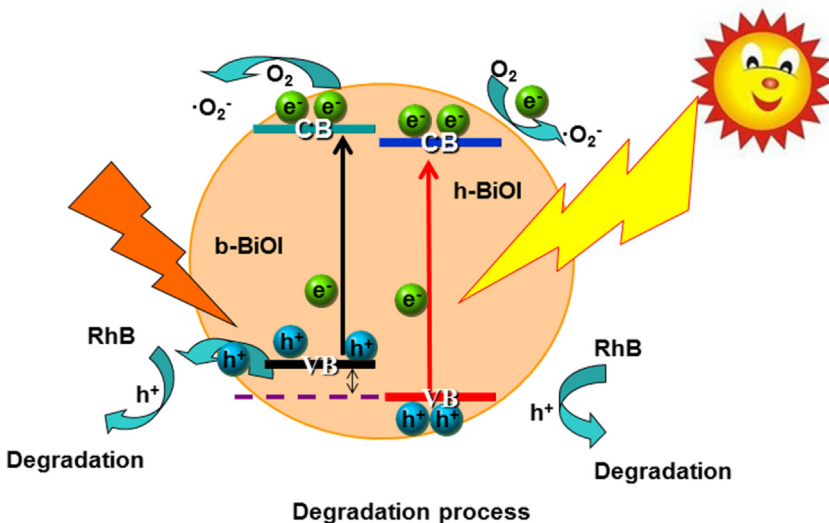


**Fig. 8.** Schematic illustration of showing the energy band structures and the electron-hole pairs separation in b-BiOI and h-BiOI.

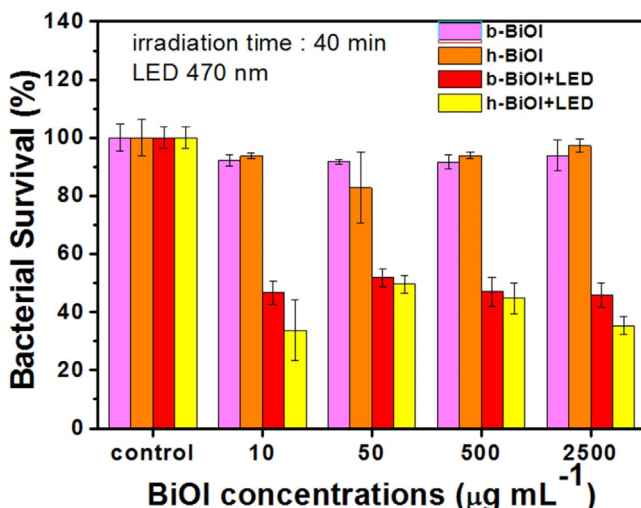


**Fig. 7.** Disinfection efficiency of *E. coli* by different concentrations of b-BiOI and h-BiOI photocatalysts under LED (470 nm) light irradiation for 40 min.

**Fig. 8**, when BiOI is irradiated by visible light, electrons are excited into the CB, leaving holes in the VB. The photo-generated electrons on CB are trapped by molecular oxygen adsorbed on the surface of BiOI to form superoxide ions ( $O_2^-$ ). In addition, the photo-generated holes on VB are able to directly oxidize RhB. It is observed that the VB position of h-BiOI obviously positive shift compared with that of b-BiOI, which indicates the holes of h-BiOI have stronger oxidation ability than that of b-BiOI. This may be the major reason that h-BiOI can completely degrade RhB while b-BiOI could only decompose RhB into segmental fragments. Moreover, it is much faster for the photogenerated charge carriers to reach the surface of h-BiOI than that of b-BiOI, which lead to more efficient separation of photo-generated electrons and holes in h-BiOI. This may be another reason for the better photocatalytic activity of h-BiOI. Besides that, the high BET surface area of h-BiOI also plays an important role in the enhancement of photocatalytic activity.

#### 4. Conclusions

In this work, hollow flower like BiOI consisting of ultrathin nanosheet was synthesized via a facile solvothermal method. The ultrathin nanosheet is confirmed by TEM. The obtained h-BiOI

exhibits improved photocatalytic activity, complete decomposition of the RhB under visible light irradiation and also efficient bactericidal activity. The origin of excellent photocatalytic activity of h-BiOI is ultrathin nanosheet, which results in large BET surface area, positive shift of VB band, and efficient separation of photogenerated charge carriers.

#### Acknowledgments

This work was financially supported by a research Grant from the National Basic Research Program of China (the 973 Program, No. 2013CB632401), the National Natural Science Foundation of China (Nos. 21333006, 21573135, 11374190, 51002091, 21007031), Taishan Scholar Foundation of Shandong Province, China, Young Scholars Program of Shandong University (2016WLJH16) and the Shandong Province Natural Science Foundation (ZR2014JL008). The authors thank Prof. Zhanjun Gu (institute of high energy physics Chinese academy of Sciences) for the disinfection experiments on *Escherichia coli* (*E. coli*).

#### Appendix A. Supplementary data

Supplementary data associated with this article can be found, in the online version, at <http://dx.doi.org/10.1016/j.apcatb.2017.03.072>.

#### References

- [1] P. Zhang, M. Fujitsuka, T. Majima, *Appl. Catal. B: Environ.* 185 (2016) 181–188.
- [2] S.Q. Jiang, L. Wang, W.C. Hao, W.X. Li, H.J. Xin, W.W. Wang, T.M. Wang, *J. Phys. Chem. C* 119 (2015) 14094–14101.
- [3] Y. Qu, X. Duan, *Chem. Soc. Rev.* 42 (2013) 2568–2580.
- [4] B. Xue, T.S. Wu, J.K. Wu, F. Mao, W. Yang, *Ultrason. Sonochem.* 22 (2015) 1–6.
- [5] W. Wang, G. Huang, J.C. Yu, P.K. Wong, *J. Environ. Sci.* 34 (2015) 232–247.
- [6] Z.Y. Jiang, Y.Y. Liu, T. Jing, B.B. Huang, Z.Y. Wang, X.Y. Zhang, X.Y. Qin, Y. Dai, *Appl. Catal. B: Environ.* 200 (2017) 230–236.
- [7] L. Guo, C. Shan, J. Liang, J. Ni, M. Tong, *Colloid Surf. B: Biointerfaces* 128 (2015) 211–218.
- [8] H.F. Cheng, M.C. Wen, X.C. Ma, Y. Kuwahara, K. Mori, Y. Dai, B.B. Huang, H. Yamashita, *J. Am. Chem. Soc.* 138 (2016) 9316–9324.
- [9] B. Zhang, Z.Y. Wang, B.B. Huang, X.Y. Zhang, X.Y. Qin, H.L. Li, Y. Dai, Y.J. Li, *Chem. Mater.* 28 (2016) 6613–6620.
- [10] T.K. Townsend, E.M. Sabio, N.D. Browning, F.E. Osterloh, *Energy Environ. Sci.* 4 (2011) 4270–4275.
- [11] J.G. Hou, H.J. Cheng, O. Takeda, H.M. Zhu, *Energy Environ. Sci.* 8 (2015) 1348–1357.
- [12] Y.F. Zhao, X.D. Jia, G.I.N. Waterhouse, L.Z. Wu, C.H. Tung, D.O. Hare, T.R. Zhang, *Adv. Energy Mater.* 6 (2016) 1501974.

- [13] S. Ghosh, N.A. Kouame, L. Ramos, S. Remita, A. Dazzi, A.D. Besseau, P. Beaunier, F. Goubard, P.H. Aubert, H. Remita, *Nat. Mater.* 14 (2015) 505–511.
- [14] Y.F. Zhao, G.B. Chen, T. Bian, C. Zhou, G.I.N. Waterhouse, L.Z. Wu, C.H. Tung, L.J. Smith, D.O. Hare, T.R. Zhang, *Adv. Mater.* 27 (2015) 7824–7831.
- [15] S.U. Khan, M.M. Al-Shahry, W.B. Ingler Jr., *Science* 297 (2002) 2243–2245.
- [16] M.R. Hoffmann, S.T. Martin, W. Choi, D.W. Bahnemann, *Chem. Rev.* 95 (1995) 69–96.
- [17] Z. Jiang, F. Yang, N. Luo, B.T.T. Chu, D. Sun, H. Shi, T. Xiao, P.P. Edwards, *Chem. Commun.* (2008) 6372–6374.
- [18] L. Shang, B. Tong, H.J. Yu, G.I.N. Waterhouse, C. Zhou, Y.F. Zhao, M. Tahir, L.Z. Wu, C.H. Tung, T.R. Zhang, *Adv. Energy Mater.* 6 (2016) 1501241.
- [19] Y.F. Zhao, B. Zhao, J.J. Liu, G.B. Chen, R. Gao, S.Y. Yao, M.Z. Li, Q.H. Zhang, L. Gu, J.L. Xie, X.D. Wen, L.Z. Wu, C.H. Tung, D. Ma, T.R. Zhang, *Angew. Chem. Int. Ed.* 55 (2016) 4215–4219.
- [20] J. Shang, W.C. Hao, X.J. Lv, T.M. Wang, X.L. Wang, Y. Du, S.X. Dou, T.F. Xie, D.J. Wang, J.O. Wang, *ACS. Catal.* 4 (2014) 954–961.
- [21] H.F. Feng, Z.F. Xu, L. Wang, Y.X. Yu, D. Mitchell, D.D. Cui, X. Xu, J. Shi, T. Sannomiya, Y. Du, W.C. Hao, S.X. Dou, *ACS Appl. Mater. Interfaces* 7 (2015) 27592–27596.
- [22] H.F. Cheng, B.B. Huang, Y. Dai, *Nanoscale* 6 (2014) 2009–2026.
- [23] J. Li, Y. Yu, L.Z. Zhang, *Nanoscale* 6 (2014) 8473–8488.
- [24] H.W. Huang, K. Xiao, Y. He, T.R. Zhang, F. Dong, X. Du, Y.H. Zhang, *Appl. Catal. B: Environ.* 199 (2016) 75–86.
- [25] H. Liu, W.R. Cao, Y. Su, Y. Wang, X.H. Wang, *Appl. Catal. B: Environ.* 112 (2012) 271–279.
- [26] Y.F. Liu, W.Q. Yao, D. Liu, R.L. Zong, M. Zhang, X.G. Ma, Y.F. Zhu, *Appl. Catal. B: Environ.* 163 (2015) 547–553.
- [27] C.X. Liao, Z.J. Ma, X.F. Chen, X. He, J.R. Qiu, *Appl. Surf. Sci.* 387 (2016) 1247–1256.
- [28] X.N. Wang, W.L. Bi, P.P. Zhai, X.B. Wang, H.J. Li, G. Mailhot, W.B. Dong, *Appl. Surf. Sci.* 360 (2016) 240–251.
- [29] R.G. He, J.F. Zhang, J.G. Yu, S.W. Cao, *J. Colloid Interface Sci.* 478 (2016) 201–208.
- [30] S.Q. Han, J. Li, K.L. Yang, J. Lin, *Chin. J. Catal.* 36 (2015) 2119–2126.
- [31] X.J. Wang, F.T. Li, D.Y. Li, R.H. Liu, S.J. Liu, *Mater. Sci. Eng. B* 193 (2015) 112–120.
- [32] J. Di, J.X. Xia, M.X. Ji, L. Xu, S. Yin, Z.G. Chen, H.M. Li, *J. Mater. Chem. A* 4 (2016) 5051–5061.
- [33] X. Zhang, B.H. Li, J.L. Wang, Y. Yuan, Q.J. Zhang, Z.Z. Gao, L.M. Liu, L. Chen, *Phys. Chem. Chem. Phys.* 16 (2014) 25854–25861.
- [34] J.L. Liang, C. Shan, X. Zhang, M.P. Tong, *Chem. Eng. J.* 279 (2015) 277–285.
- [35] H.F. Cheng, W.J. Wang, B.B. Huang, Z.Y. Wang, J. Zhan, X.Y. Qin, X.Y. Zhang, Y. Dai, *J. Mater. Chem. A* 1 (2013) 7131–7136.
- [36] F. Dong, Y. Sun, M. Fu, Z. Wu, S.C. Lee, *J. Hazard. Mater.* 219 (2012) 26–34.
- [37] Z.H. Ai, W.K. Ho, S.C. Lee, L.Z. Zhang, *Environ. Sci. Technol.* 43 (2009) 4143–4150.
- [38] C. Liu, X.J. Wang, *Dalton Trans.* 45 (2016) 7720–7727.
- [39] L. Chen, S.F. Yin, R. Huang, Q. Zhang, S.L. Luo, C.T. Au, *CrystEngComm* 14 (2012) 4217–4222.